Current Biology, Volume *36*

Supplemental Information

Genomic and physiological changes in a sexually selected and frugivorous bird radiation

Christopher N. Balakrishnan, Yasuka Toda, Meng-Ching Ko, Morgan E. Wirthlin, Robert J. Driver, Peri E. Bolton, Eliot T. Miller, Daniel Mendez-Aranda, Rebecca B. Dikow, Paul B. Frandsen, Elsie H. Shogren, Kevin F.P. Bennett, H. Luke Anderson, Madeline G. Bursell, Julia F. Cramer, Keren R. Sadanandan, Tomoya Nakagita, Marco A. Pizo, Daniel S. Caetano, Marina Anciães, Carolina F. Ferreira, Jacob S. Berv, Kira M. Long, Haw Chuan Lim, Andre E. Moncrieff, Sarah E. Kingston, Noor D. White Carreiro, Samantha R. Friedrich, Camilo Alfonso Cuta, James B. Pease, Alexander A. Nevue, Chad Tomlinson, Aleksey Zimin, Matthew I.M. Louder, Michael S. Brewer, Rachael A. Bay, Kristen Ruegg, Thomas B. Smith, Yoshiro Ishimaru, Andreas R. Pfenning, Carolina Frankl-Vilches, Manfred Gahr, Claudio V. Mello, Rebecca T. Kimball, Edward L. Braun, John G. Blake, Lainy B. Day, T. Brandt Ryder, Ignacio T. Moore, Brent M. Horton, Barney A. Schlinger, Matthew J. Fuxjager, Wesley C. Warren, Emily H. DuVal, W. Alice Boyle, Bette A. Loiselle, Michael J. Braun, and Maude W. Baldwin

Current Biology, Volume *36*

Supplemental Information

Genomic and physiological changes in a sexually selected and frugivorous bird radiation

Christopher N. Balakrishnan, Yasuka Toda, Meng-Ching Ko, Morgan E. Wirthlin, Robert J. Driver, Peri E. Bolton, Eliot T. Miller, Daniel Mendez-Aranda, Rebecca B. Dikow, Paul B. Frandsen, Elsie H. Shogren, Kevin F.P. Bennett, H. Luke Anderson, Madeline G. Bursell, Julia F. Cramer, Keren R. Sadanandan, Tomoya Nakagita, Marco A. Pizo, Daniel S. Caetano, Marina Anciaes, Carolina F. Ferreira, Jacob S. Berv, Kira M. Long, Haw Chuan Lim, Andre E. Moncrieff, Sarah E. Kingston, Noor D. White Carreiro, Samantha R. Friedrich, Camilo Alfonso Cuta, James B. Pease, Alexander A. Nevue, Chad Tomlinson, Aleksey Zimin, Matthew I.M. Louder, Michael S. Brewer, Rachael A. Bay, Kristen Ruegg, Thomas B. Smith, Yoshiro Ishimaru, Andreas R. Pfenning, Carolina Frankl-Vilches, Manfred Gahr, Claudio V. Mello, Rebecca T. Kimball, Edward L. Braun, John G. Blake, Lainy B. Day, T. Brandt Ryder, Ignacio T. Moore, Brent M. Horton, Barney A. Schlinger, Matthew J. Fuxjager, Wesley C. Warren, Emily H. DuVal, W. Alice Boyle, Bette A. Loiselle, Michael J. Braun, and Maude W. Baldwin

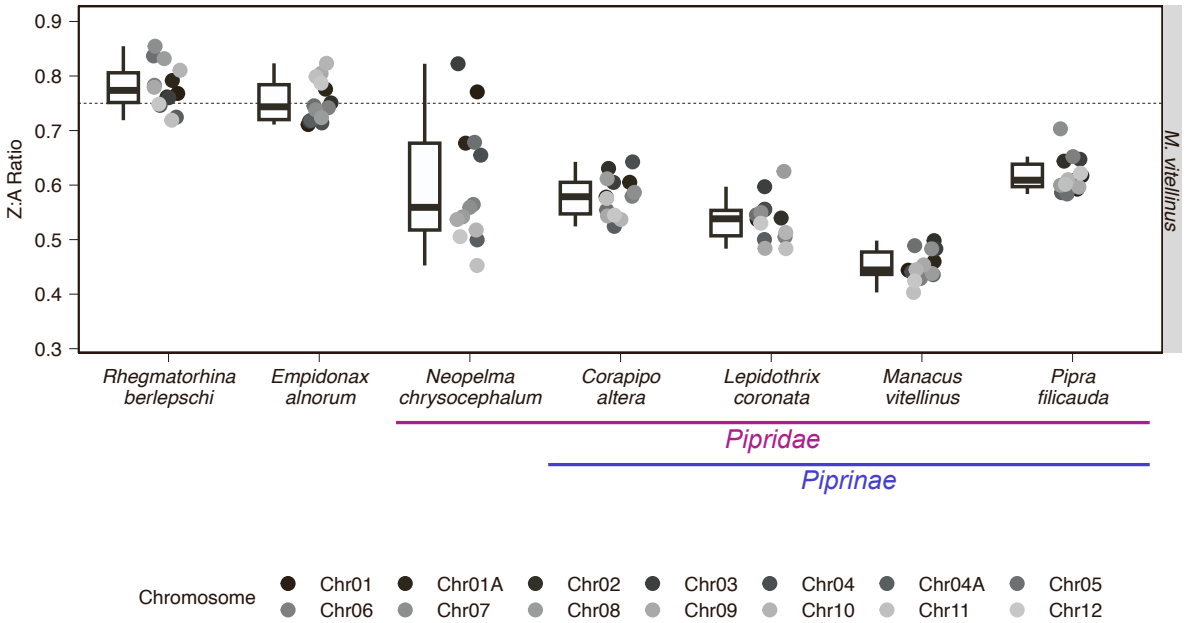
Z:A Ratio
0.9
0.8
0.7
0.6
0.5
0.4
0.3
M. vitellinus
Rhegmatorhina berlepschi
Empidonax alnorum
Neopelma chrysocephalum
Corapipo altera
Lepidothrix coronata
Manacus vitellinus
Pipra filicauda
Pipridae
Piprinae

Chromosome
Chr01
Chr01A
Chr02
Chr03
Chr04
Chr04A
Chr05
Chr06
Chr07
Chr08
Chr09
Chr10
Chr11
Chr12

Figure S1. Estimates of relative genetic diversity on the Z chromosome versus autosomes. Related to Figure 1. Patterns of genetic diversity on the Z chromosome (Figure 1E) are not affected by mapping to different assemblies. Here, the *M. vitellinus* was selected as the reference (in Figure 1E, RADseq data from each manakin were mapped to the species' respective assembly). Boxplots illustrate genetic diversity on the Z chromosome relative to each autosome, indicating the 25^{th}, 50^{th}, and 75^{th} percentiles.

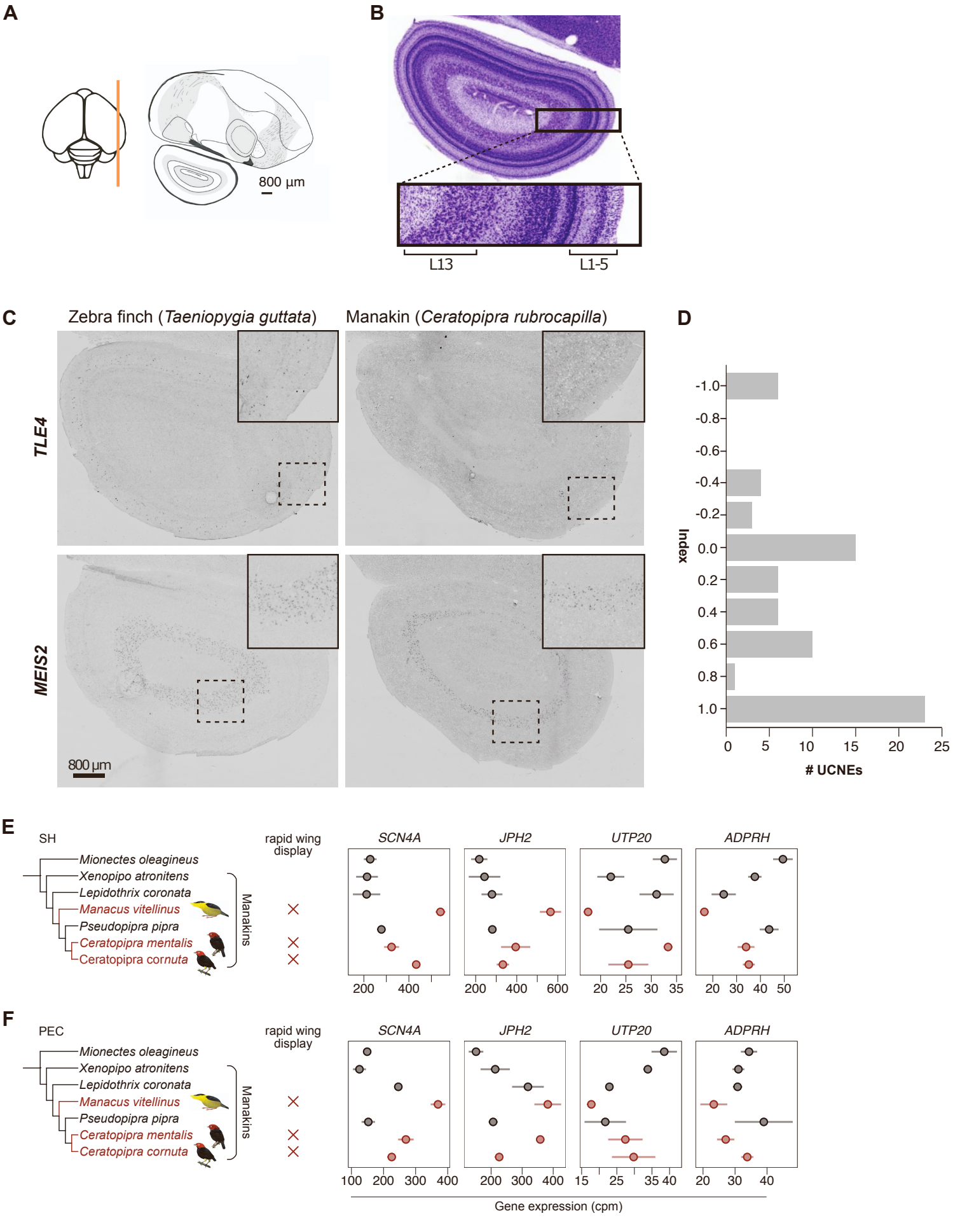
A
800 µm
B
L13
L1-5
C
Zebra finch (Taeniopygia guttata)
Manakin (Ceratopipra rubrocapilla)
TLE4
MEIS2
800 µm
D
Index
-1.0
-0.8
-0.6
-0.4
-0.2
0.0
0.2
0.4
0.6
0.8
1.0
0
5
10
15
20
25
UCNEs
E
SH
rapid wing display
Mionectes oleagineus
Xenopipo atronitens
Lepidothrix coronata
Manacus vitellinus
Pseudopipra pipra
Ceratopipra mentalis
Ceratopipra cornuta
Manakins
SCN4A
JPH2
UTP20
ADPRH
F
PEC
rapid wing display
Mionectes oleagineus
Xenopipo atronitens
Lepidothrix coronata
Manacus vitellinus
Pseudopipra pipra
Ceratopipra mentalis
Ceratopipra cornuta
Manakins
SCN4A
JPH2
UTP20
ADPRH
Gene expression (cpm)

Figure S2. UCNE analyses and changes in loci potentially related to perception and production of displays. Related to Figure 2. A-C): Manakin-accelerated UCNEs and midbrain expression patterns of two transcription factors (*TLE4* and *MEIS2*) proximal to accelerated UCNEs. Single-color *in situ* hybridization reveals that *TLE4* and *MEIS2* are expressed in specific layers of the optic tectum in both an adult male zebra finch and a red-headed manakin (*Ceratopipra rubrocapilla*). A) Line drawing of a zebra finch parasagittal brain section at the location analyzed; illustration of dorsal brain view depicts location of the sections analyzed (orange bar). B) Photomicrograph of a Nissl-stained brain section (drawn in A) through the optic tectum; the zoomed-in view in the rectangle inset depicts stained tectal layers (L1-5 and L13 are indicated). A-B adapted from images presented in Figures 2 and 8 of[S1], reproduced with permission. C) *In situ* hybridizations of brain sections of a zebra finch and a red-headed manakin, at the level shown in A-B. *TLE4* expression was seen in sparse cells of superficial tectal layers (L1-5) in both species (top panels; insets in top right corners depict zoomed-in views of the boxed regions), which are thought to be the main tectal input layers from the retina. *MEIS2* expression was strong in deep layer 13 (L13), a.k. *stratum griseum centrale* (bottom panels; insets in top right corners depict zoomed-in views of the boxed regions), which contains motion-sensitive neurons and is thought to be the main source of the output tectofugal projection to thalamic nucleus rotundus. The patterns were similar in both species; further study would be needed to establish possible quantitative species differences. The avian optic tectum is considered homologous to the mammalian superior colliculus[S2]. This highly layered midbrain structure receives non-thalamic retinal input and plays prominent and conserved roles in visual motion detection and head and eye orientation reflexes[S3–5]. TLE4 and MEIS2 play closely related roles in tectal development[S6]. Overall, these findings suggest that tectal pathways for visual motion detection and head orientation may play a role in tracking the elaborate acrobatic courtship displays of manakins, to be further tested in future studies. D) Out of 74 of manakin-accelerated UCNEs (63 associated with genes), 14 exhibit more changes on the branch leading to the Piprinae clade (negative index values) relative to the branch leading to all manakins (Pipridae); 46 UCNEs have index values > 0 indicating more change on the branch leading to the manakin radiation. The index is calculated as (# changes on the Pipridae branch- # changes on the Piprinae branch/(# changes on the Pipridae branch + # changes on the Piprinae branch). E-F) Positively-selected muscle genes show expression changes in different manakin species. A subset of muscle-related genes that are under positive selection in the MK test also show evidence of expression changes associated with the evolution of rapid wing displays (such as the ‘wing-snaps' performed by *Manacus vitellinus)* relative to other manakins). Results are shown for two flight muscles, *scapulohumeralis caudalis* (SH, panel E) and *pectoralis* (PEC, panel F); SH is a ‘superfast’ forelimb muscle modified for display performance in some manakins. We identified a subset of genes that showed evidence for change in the SH muscle (BayesFactor > 0.4) in *Manacus* or shared changes in *Manacus* and *Ceratopipra* (MCC model, see[S7]). Values represent mean ± SE.

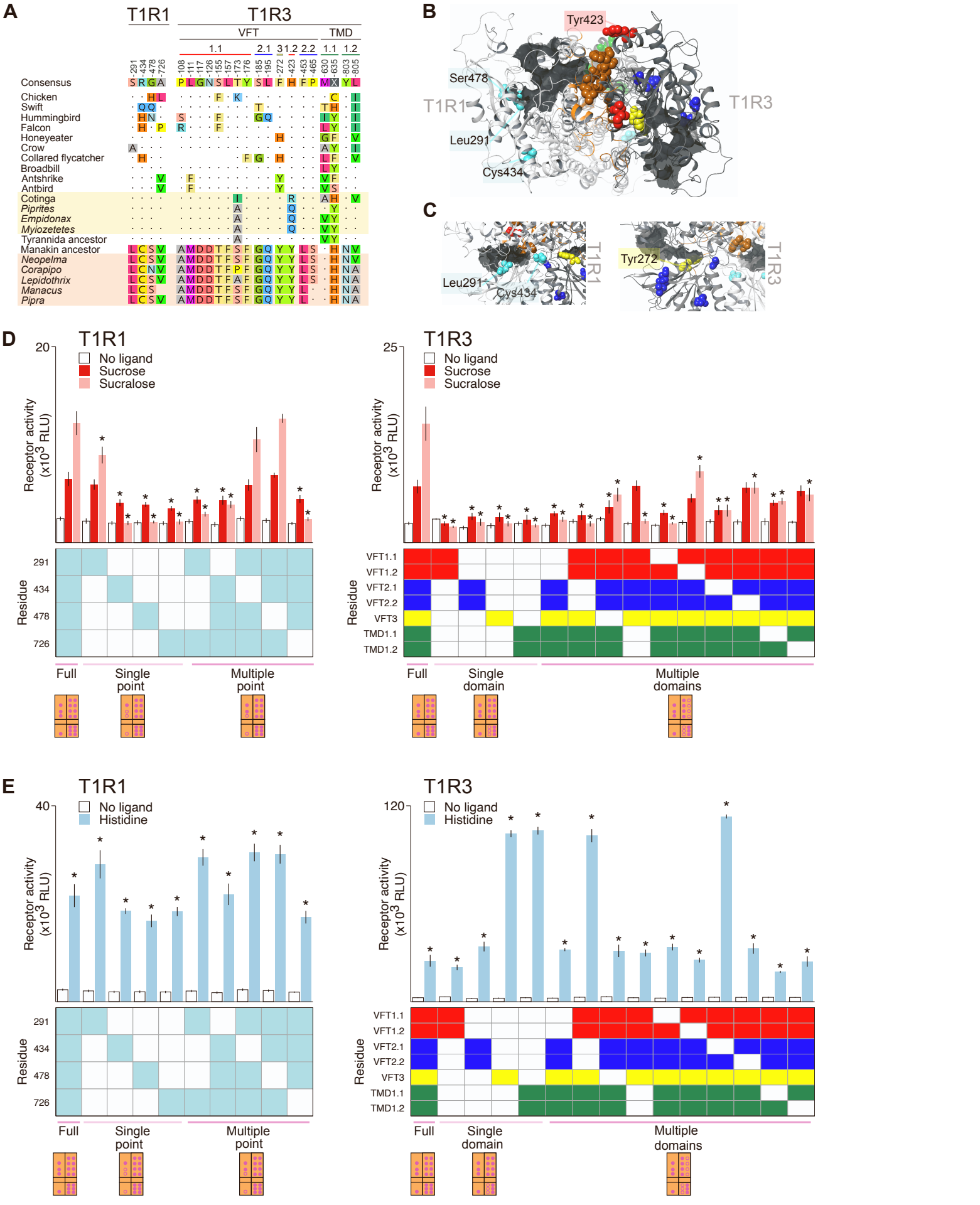
A
T1R1
T1R3
VFT
TMD
1.1
2.1
3
1.2
2.2
1.1
1.2
291 434 478 726 108 111 117 126 155 157 173 176 185 195 272 423 453 465 630 635 803 805
Consensus S R G A P L G N S L T Y S L F H F P M X Y L
Chicken H L F K C I
Swift Q Q T T H I
Hummingbird H N S F G Q I Y I
Falcon H P R F L Y I
Honeyeater H G F V
Crow A A Y I
Collared flycatcher H F G H L F V
Broadbill L Y
Antshrike V F Y V F
Antbird V F Y V S
Cotinga I R A H V
Piprites A Q Y
Empidonax A Q V Y
Myiozetetes A Q V Y
Tyrannida ancestor A V Y
Manakin ancestor L C S V A M D D T F S F G Q Y Y L S H N V
Neopelma L C S V A M D D T F S F G Q Y Y L S H N V
Corapipo L C N V A M D D T F P F G Q Y Y L S H N A
Lepidothrix L C S V A M D D T F A F G Q Y Y L S H N A
Manacus L C S A M D D T F S F G Q Y Y L H N A
Pipra L C S V A M D D T F S F G Q Y Y L H N A
B
Tyr423
Ser478
T1R1
T1R3
Leu291
Cys434
C
T1R1
Leu291
Cys434
Tyr272
T1R3
D
T1R1
No ligand
Sucrose
Sucralose
Receptor activity (x10^3 RLU)
Residue
291
434
478
726
Full
Single point
Multiple point
T1R3
No ligand
Sucrose
Sucralose
Receptor activity (x10^3 RLU)
Residue
VFT1.1
VFT1.2
VFT2.1
VFT2.2
VFT3
TMD1.1
TMD1.2
Full
Single domain
Multiple domains
E
T1R1
No ligand
Histidine
Receptor activity (x10^3 RLU)
Residue
291
434
478
726
Full
Single point
Multiple point
T1R3
No ligand
Histidine
Receptor activity (x10^3 RLU)
Residue
VFT1.1
VFT1.2
VFT2.1
VFT2.2
VFT3
TMD1.1
TMD1.2
Full
Single domain
Multiple domains

Figure S3. Chimeric analysis reveals critical residues in T1R1 and T1R3. Related to Figure 3. A) Four amino acid residues in T1R1 affect the response to sucrose and sucralose; 18 residues are necessary in T1R3. Residues from the two ancestral reconstructions (Tyrannida ancestor and manakin ancestor inferred from an alignment with 31 taxa, see Methods) used for chimeric dissection are depicted. For comparison, residues are shown from other taxa included in selection tests; manakins are highlighted in pale orange, other members of the Tyrannida are highlighted in yellow. B) View from top of VFT domains of T1R1-T1R3 heterodimer shows relative location of critical residues (binding pocket in grey). C) L291 (in T1R1) and Y272 (in T1R3) are located in the binding pocket. D) Analysis of chimeric receptors: in addition to 291, T1R1 critical residues 434 and 478 are also in the Venus fly-trap (VFT) domain, and 726 is in the transmembrane domain (see Figure 3); epistasis is seen in tests of residue combinations. In T1R3, both the VFT and TM domains are involved; interestingly, distinct residue subsets are required for response to sucrose and sucralose: absence of residues in VFT1.2, VFT2.2, and TM1.2 affects sucralose responses but not sucrose responses. 6 residues (D117, D126, T155, F157, S173, F176) in VFT1.1 are within 4 angstroms of T1R1 and are colored brown in Figure 3G; the remaining two residues in VFT1.1 (A108 and M111) and a residue in VFT1.2 (Y423) are not within 4 angstroms but are near the brown residues. VFT3 is residue 272, in the orthosteric binding pocket. How the blue residues in the VFT (as well as the residues in the transmembrane domain) affect receptor function is not yet known. Interestingly, some of the sites in T1R3 are also close to sites (in both T1R1 or T1R3) identified in other studies: M111 corresponds to site C106 of the ancestral songbird T1R1[S8]; similarly, D117 and T155 of manakin T1R3 are adjacent to R113 and S149 of the ancestral songbird T1R1. In addition, manakin T1R3 Y272 is next to human T1R1 site R277, reported as the binding site of inosine monophosphate (IMP)[S9], and manakin T1R3 sites M630 and H635 are close to or correspond to key residues of the ancestral songbird T1R3, as well as to the binding sites of NHDC, cyclamate and lactisole in human T1R3[S10–12]. Of the four identified sites in manakin T1R1, L291 is also close to sites in human T1R1 involved in nucleotide and glutamate binding. Here, for comparison (and in contrast to Figure 3), asterisks indicate decreased responses compared to the 'full' chimera (with 4 T1R1 residues and 18 T1R3 residues); n = 6; mean ± SE; * $p < 0.05$, Welch's one-tailed t-test, FDR adjustment for multiple comparisons. E) Histidine responses indicate functionality of tested chimeric responses; all responses are significantly different than no-ligand controls (n = 6; mean ± SE; *$p < 0.05$, Welch's one-tailed t-test, FDR; respective no ligand controls are the same as shown in D). Some chimeric receptors (especially those lacking the manakin ancestral sequence at VFT2.1) exhibit dramatically enhanced responses compared to the full chimera, indicating that similar regions may affect responses to both amino acids and sugars.

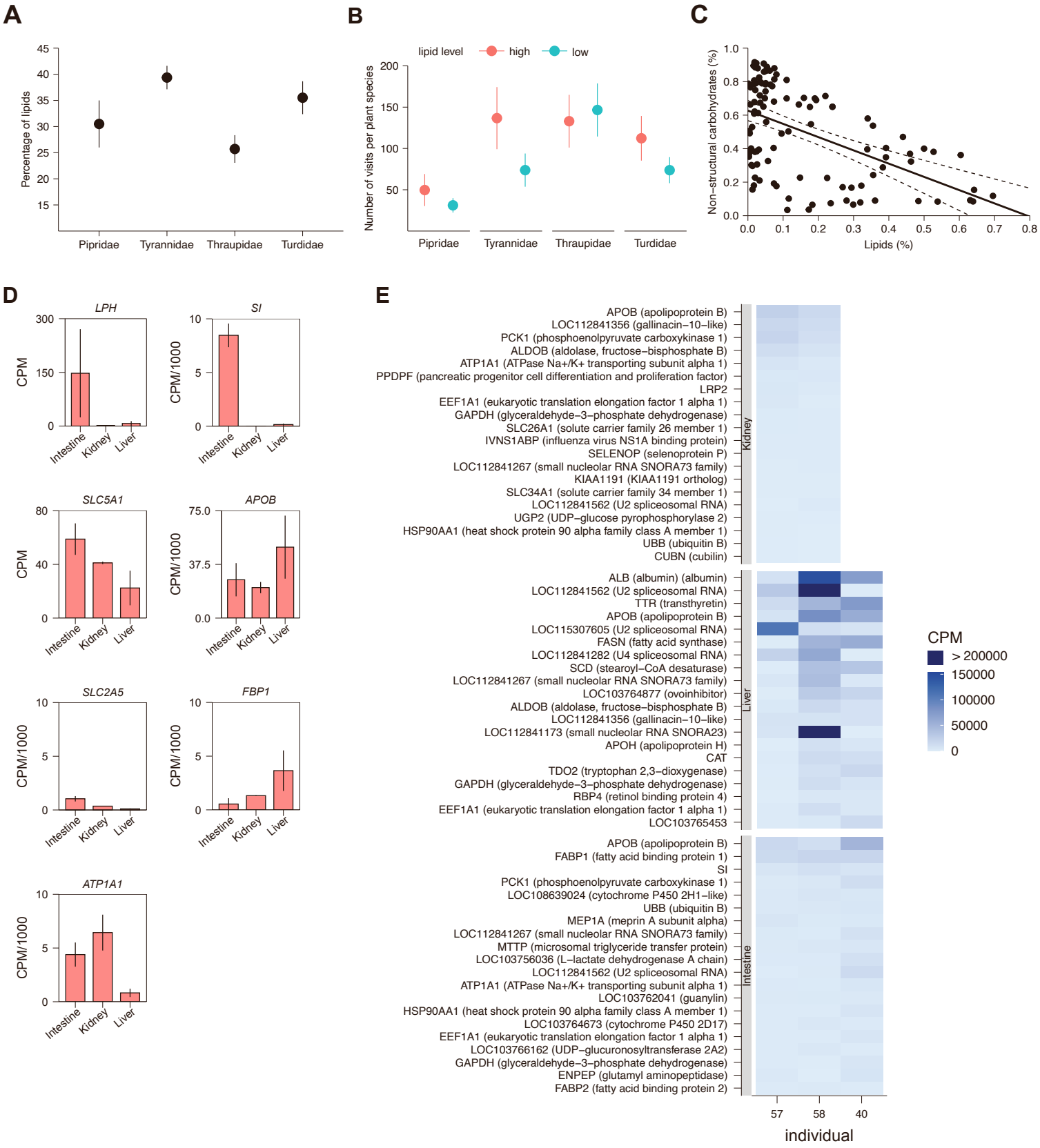
A
Percentage of lipids
Pipridae
Tyrannidae
Thraupidae
Turdidae
B
lipid level
high
low
Number of visits per plant species
C
Non−structural carbohydrates (%)
Lipids (%)
D
LPH
SI
SLC5A1
APOB
SLC2A5
FBP1
ATP1A1
CPM
CPM/1000
Intestine
Kidney
Liver
E
APOB (apolipoprotein B)
LOC112841356 (gallinacin−10−like)
PCK1 (phosphoenolpyruvate carboxykinase 1)
ALDOB (aldolase, fructose−bisphosphate B)
ATP1A1 (ATPase Na+/K+ transporting subunit alpha 1)
PPDPF (pancreatic progenitor cell differentiation and proliferation factor)
LRP2
EEF1A1 (eukaryotic translation elongation factor 1 alpha 1)
GAPDH (glyceraldehyde−3−phosphate dehydrogenase)
SLC26A1 (solute carrier family 26 member 1)
IVNS1ABP (influenza virus NS1A binding protein)
SELENOP (selenoprotein P)
LOC112841267 (small nucleolar RNA SNORA73 family)
KIAA1191 (KIAA1191 ortholog)
SLC34A1 (solute carrier family 34 member 1)
LOC112841562 (U2 spliceosomal RNA)
UGP2 (UDP−glucose pyrophosphorylase 2)
HSP90AA1 (heat shock protein 90 alpha family class A member 1)
UBB (ubiquitin B)
CUBN (cubilin)
Kidney
ALB (albumin) (albumin)
LOC112841562 (U2 spliceosomal RNA)
TTR (transthyretin)
APOB (apolipoprotein B)
LOC115307605 (U2 spliceosomal RNA)
FASN (fatty acid synthase)
LOC112841282 (U4 spliceosomal RNA)
SCD (stearoyl−CoA desaturase)
LOC112841267 (small nucleolar RNA SNORA73 family)
LOC103764877 (ovoinhibitor)
ALDOB (aldolase, fructose−bisphosphate B)
LOC112841356 (gallinacin−10−like)
LOC112841173 (small nucleolar RNA SNORA23)
APOH (apolipoprotein H)
CAT
TDO2 (tryptophan 2,3−dioxygenase)
GAPDH (glyceraldehyde−3−phosphate dehydrogenase)
RBP4 (retinol binding protein 4)
EEF1A1 (eukaryotic translation elongation factor 1 alpha 1)
LOC103765453
Liver
APOB (apolipoprotein B)
FABP1 (fatty acid binding protein 1)
SI
PCK1 (phosphoenolpyruvate carboxykinase 1)
LOC108639024 (cytochrome P450 2H1−like)
UBB (ubiquitin B)
MEP1A (meprin A subunit alpha)
LOC112841267 (small nucleolar RNA SNORA73 family)
MTTP (microsomal triglyceride transfer protein)
LOC103756036 (L−lactate dehydrogenase A chain)
LOC112841562 (U2 spliceosomal RNA)
ATP1A1 (ATPase Na+/K+ transporting subunit alpha 1)
LOC103762041 (guanylin)
HSP90AA1 (heat shock protein 90 alpha family class A member 1)
LOC103764673 (cytochrome P450 2D17)
EEF1A1 (eukaryotic translation elongation factor 1 alpha 1)
LOC103766162 (UDP−glucuronosyltransferase 2A2)
GAPDH (glyceraldehyde−3−phosphate dehydrogenase)
ENPEP (glutamyl aminopeptidase)
FABP2 (fatty acid binding protein 2)
Intestine
CPM
> 200000
150000
100000
50000
0
57
58
40
individual

Figure S4. Data on manakin diets and expression data from *Manacus vitellinus* intestine, kidney and liver. Related to Figure 4. A) Manakins consume fruits that are both lipid-rich and lipid-poor. A) The average weighted lipid content of the fruits eaten by piprids and tyrannids, as well as two oscine frugivores (thraupids and turdids), expressed as a percent on a dry mass basis and weighted by the number of visits to fruiting plants, was calculated from a recently-published study[S13], (mean and SEM of weighted percentages shown). The number of plant and bird species included in the dataset for each bird family were, respectively: Pipridae (28/15), Thraupidae (58/55) Turdidae (50/12), Tyrannidae (50/52). A total of 19508 visits to fruiting plants were considered, distributed as follows: Pipridae (1131), Thraupidae (8093) Turdidae (4689), Tyrannidae (5513). B) Average number of feeding visits per plant species to lipid-rich and lipid-poor fruits across the four families (lipid-rich defined as fruits with lipid content in a dry mass basis ≥ 10%, lipid-poor are fruits with < 10% lipids) (mean and SEM, total visits per plant species, separated by lipid class). C) A negative correlation between fat and sugar content in fruits has been documented in other studies[S14–17]; in our dataset on Neotropical plant species, we observe this as well ($r = -0.51$, $n = 108$, $p < 0.001$). D) Expression counts across tissue type of four diet-related genes (identified in positive selection analyses). Transcriptomes from tissues of three individuals (two adult females and one juvenile) were analyzed for the liver and the intestine; the juvenile sample was omitted for kidney. High expression was seen in genes involved in both lipid and carbohydrate metabolism, such as *APOB* and *SI*; *FBP1* (under strong selection in aBSREL screens) was expressed most highly in the liver. Low but detectable expression was observed for both lactase (*LPH*) as well as *SLC5A1*; both are most highly expressed in the intestine. *LPH* counts vary across individuals: individual 58 (an adult female) had ~10 fold higher expression levels in the intestine and the liver, but not in the kidney, compared to the other two birds. Expression counts of *SLC2A5* were also higher in the intestine compared to other tissues, and *ATP1A1* was highly expressed in all tissues with highest counts in the kidney. Expression levels are expressed as counts per million (CPM), calculated as reads per kilobase (RPK; raw reads/gene length) normalized for sequencing depth. Counts of highly expressed genes are divided by 1000 (CPM/1000). Values represent mean ± SE. E) The top twenty most highly expressed genes per tissue type are shown (plotted from highest to lowest per tissue). Some genes identified as under positive selection are also highly expressed, including sucrase isomaltase (*SI*) in intestine, *APOB* and *ATP1A1* in all tissues, and *FABP2* in intestine. Albumin (*ALB*), the most highly expressed gene in the liver, exhibited a signature of selection in *Manacus*. Aldolase, fructose-bisphosphate B (*ALDOB*), identified in another study examining convergence in positive selection between nectarivorous bats and hummingbirds[S18], was highly expressed in liver and kidney (as well as being selected in the branch leading to Piprinae manakins, Figure 2E).

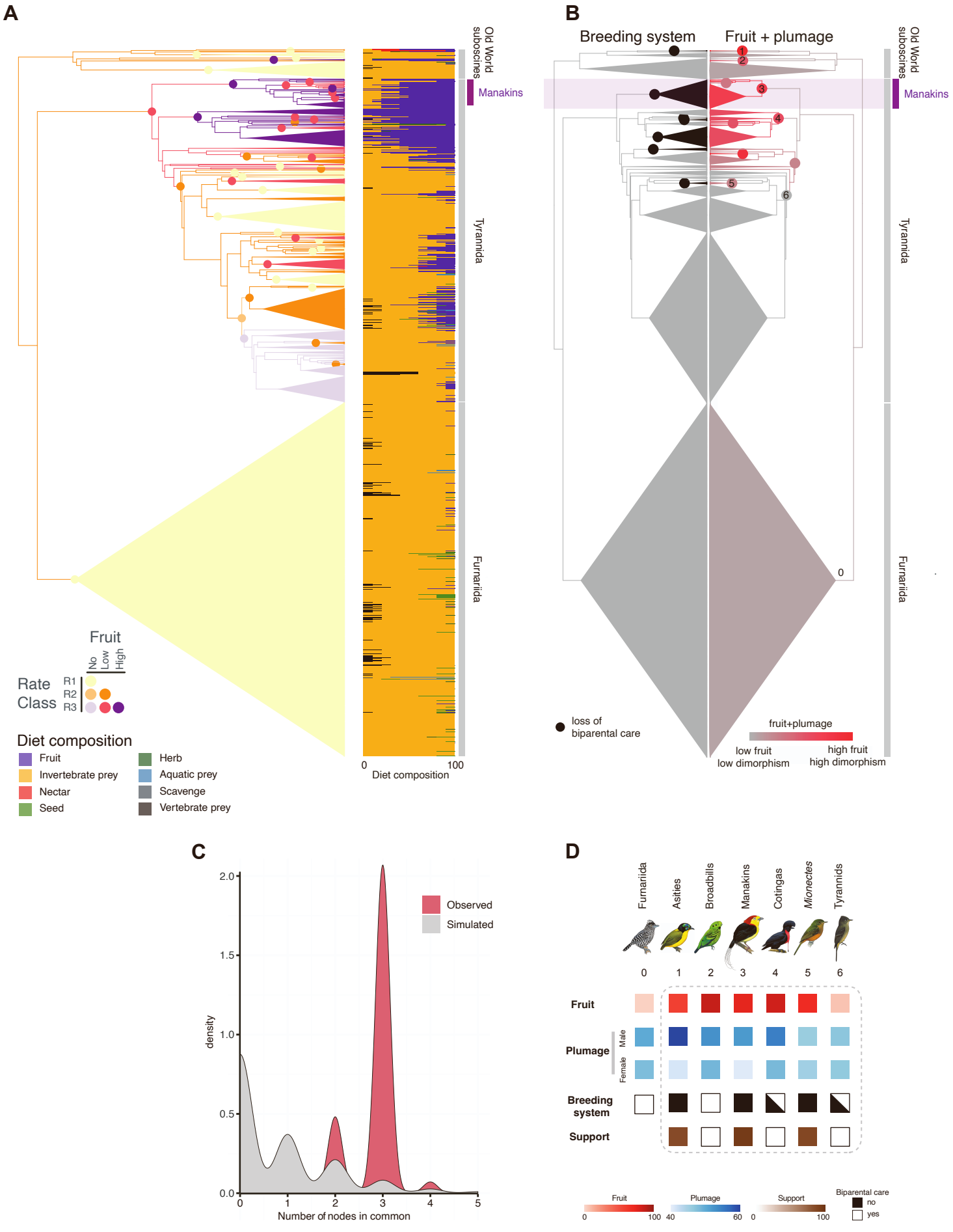
A
Old World suboscines
Manakins
Tyrannida
Furnariida
Fruit
No
Low
High
Rate Class
R1
R2
R3
Diet composition
Fruit
Invertebrate prey
Nectar
Seed
Herb
Aquatic prey
Scavenge
Vertebrate prey
0
100
Diet composition
B
Breeding system
Fruit + plumage
Old World suboscines
Manakins
Tyrannida
Furnariida
1
2
3
4
5
6
0
loss of biparental care
fruit+plumage
low fruit
low dimorphism
high fruit
high dimorphism
C
Observed
Simulated
density
2.0
1.5
1.0
0.5
0.0
0
1
2
3
4
5
Number of nodes in common
D
Furnariida
Asities
Broadbills
Manakins
Cotingas
Mionectes
Tyrannids
0
1
2
3
4
5
6
Fruit
Plumage
Male
Female
Breeding system
Support
Fruit
0
100
Plumage
40
60
Support
0
100
Biparental care
no
yes

Figure S5. Diet shifts in suboscines and associations with losses of biparental care and changes in coloration. **Related to Figure 5.** A) Reconstruction of the inferred shifts in precursor traits enabling frugivory across suboscines reveals a rate shift facilitating increased fruit consumption that evolved in the ancestor of manakins, cotingas, and tyrant flycatchers. A dual precursor model was used to examine the evolution of hidden (precursor) traits associated with shifts to high-fruit diets across suboscines. Since low levels of fruit are consumed widely across many bird clades, taxa were classified as consuming either no fruit, or low (between 10-70%) or high (> 70%) levels of fruit; high fruit consumption was only permitted in the third rate class (R3), and shifts between the first rate class (no fruit, lack of precursor trait) and the rate class enabling high fruit consumption (R3) were only permitted after transitions to the second rate class (R2; in which the precursor trait facilitating low fruit consumption had evolved). Node-specific cumulative probabilities of being in one of three rate classes (R1, R2, R3) as well as in one of three states (consuming no, low, or high fruit) were examined and shifts are color-coded and plotted on the phylogeny. A) Diet data for suboscines from[S19]; invertebrates (orange) are the predominant diet item across suboscines; manakins and cotingas consume large amounts of fruit (purple), as do some tyrant flycatchers and Old World suboscines. B) A precursor model was used to examine shifts in biparental care (black circles, predicted location of losses of biparental care) and associated shifts in frugivory and male and female coloration. The location of shifts in three continuous characters (male plumage variation, female plumage variation, and fruit, summarized by coloring clades according to their position along the first axis of a scaled and centered principal components analysis of all inferred clade optima) were determined using PhylogeneticEM and plotted on the tree on the right. Numbers on nodes refer to specific clades discussed in D. C) Kernel density plots comparing the expected (grey) and observed (red) number of coincident nodes between shifts in breeding system and shifts in fruit and plumage based on the estimated rates of transitions between states. Three strongly supported shifts (in asities, manakins, and *Mionectes*) were recovered in nearly all simulations; an additional three shifts (in broadbills, cotingas, and in other tyrant flycatchers) were occasionally recovered. D) Summary of results from our newly developed method for linking shifts in state of discrete traits with shifts in inferred optima of continuous traits. Six such coincident shifts were detected across the analysis, three of which were strongly supported, and three of which were not. The three shifts which were not well supported—*Calyptomena* broadbills, cotingas, and tyrannids—tended to occur in runs where the stochastic character mapping assigned a state of no biparental care to the root, and then a gain of biparental care was subsequently invoked by the model. Interestingly, the PhylogeneticEM model did not detect as many shifts in plumage combined with diet within the cotingas as we initially had expected (many notable shifts in breeding system within the largely frugivorous clade of cotingas do not emerge here as coincident with shifts in plumage). For example, the apparent loss of biparental care in the ancestor of the clade containing the genera *Lipaugus*, *Procnias*, *Cotinga*, and *Cephalopterus* (some members of which are strongly dimorphic), is apparently followed by subsequent gains of biparental care in *Querula purpurata* and also *Conioptilon mcilhennyi* (both of which are monomorphic). These and other interesting shifts in breeding systems within cotingas warrant further study. Bird images are reproduced with permission © Lynx

Nature Books and Cornell Lab of Ornithology (illustrated by Hilary Burn (*Thamnophilus doliatus*), John Cox (*Philepitta schlegeli*), Ian Lewington (*Calyptomena whiteheadi*), Jan Wilczur (*Pipra filicauda*), Chris Rose (*Cephalopterus glabricollis*), Brian Small (*Mionectes macconnelli*), Norman Arlott (*Contopus caribaeus*)).

Clade	Database	Term	Group	Gene	Count	List Total	Pop Hits	Pop Total	Fold Enrichment	P value	Bon-ferroni
Suboscine	GOTERM_CC_DIRECT	GO:0005903~brush border	Diet	VIL1, SLC9A3, SLC15A1, MYO1B, DAB1, MME, SI, CDHR2, MYO7B, TMPRSS15	10	591	32	7837	4.14	0.00	0.18
Suboscine	KEGG_PATHWAY	hsa04974:Protein digestion and absorption	Diet	DPP4, SLC9A3, ACE2, COL3A1, SLC15A1, CTRL, MME, SLC7A9, COL6A1, SLC3A1, ATP1A1	11	233	44	3196	3.43	0.00	0.21
Suboscine	GOTERM_CC_DIRECT	GO:0031526~brush border membrane	Diet	GNA13, SLC9A3, SLC7A9, GNA12, CDHR2, SLC3A1, SLC5A1, MFSD10	8	591	30	7837	3.54	0.01	0.93
Suboscine	GOTERM_CC_DIRECT	GO:0000781~chromosome, telomeric region	Telomere	SETX, TERT, DOT1L, DYDC2, SMC5, TP53BP1, SMC6	7	591	31	7837	2.99	0.03	1.00
Suboscine	UP_KEYWORDS	Vision	Sensory	ADGRV1, BBS10, FAM161A, CYP4V2, RGR, RGS9, EYS, SPATA7, RPGR, CNGB1	10	621	61	8240	2.18	0.04	1.00
Suboscine	UP_KEYWORDS	Spermatogenesis	Sperm	TDRD1, SETX, DAZAP1, SLCO4C1, ASZ1, TDRD12, MYCBPAP, TDRD6, SPATA20, CFAP54	10	621	66	8240	2.01	0.06	1.00
Suboscine	KEGG_PATHWAY	hsa04973:Carbohydrate digestion and absorption	Diet	HK3, SI, SLC5A1, ATP1A1, LPH	5	233	21	3196	3.27	0.06	1.00
Pipridae	KEGG_PATHWAY	hsa04974:Protein digestion and absorption	Diet	SLC9A3, COL3A1, COL15A1, CTRL, COL4A1, COL12A1, COL6A1, COL6A3, ATP1A1	9	114	44	3196	5.73	0.00	0.02
Pipridae	GOTERM_CC_DIRECT	GO:0005903~brush border	Diet	SLC9A3, SLC34A2, FLII, SI, LCTL	5	263	32	7837	4.66	0.02	1.00
Pipridae	GOTERM_CC_DIRECT	GO:0042383~sarcolemma	Muscle	COL6A1, COL6A3, CD59, ATP1A1, SLC2A5, CLCN1	6	263	48	7837	3.72	0.02	1.00
Pipridae	GOTERM_BP_DIRECT	GO:0005975~carbohydrate metabolic process	Diet	LDHB, SLC35A1, SI, LPH, NAGPA, SLC2A5, SIAE, LCTL	8	250	90	7523	2.67	0.03	1.00
Pipridae	KEGG_PATHWAY	hsa04973:Carbohydrate digestion and absorption	Diet	SI, ATP1A1, LPH, SLC2A5	4	114	21	3196	5.34	0.04	1.00
Pipridae	GOTERM_BP_DIRECT	GO:0015755~fructose transport	Diet	SLC2A5, SLC26A5	2	250	2	7523	30.09	0.07	1.00
Pipridae	GOTERM_BP_DIRECT	GO:0044245~polysaccharide digestion	Diet	SI, LPH	2	250	2	7523	30.09	0.07	1.00
Pipridae	GOTERM_BP_DIRECT	GO:0042159~lipoprotein catabolic process	Diet	ATM, APOB	2	250	2	7523	30.09	0.07	1.00
Pipridae	GOTERM_BP_DIRECT	GO:0008643~carbohydrate transport	Diet	SLC35A1, SLC35D2, SLC2A5	3	250	14	7523	6.45	0.08	1.00
Pipridae	GOTERM_CC_DIRECT	GO:0000781~chromosome, telomeric region	Telomere	TERB1, NSMCE2, ATM, TP53BP1	4	263	31	7837	3.84	0.08	1.00
Pipridae	GOTERM_BP_DIRECT	GO:0030073~insulin secretion	Diet	SNX19, GPR119, FAM3B	3	250	15	7523	6.02	0.09	1.00
Piprinae	GOTERM_CC_DIRECT	GO:0000781~chromosome, telomeric region	Telomere	TERT, SPO11, TP53BP1, NBN	4	140	31	7837	7.22	0.02	0.97
Piprinae	UP_KEYWORDS	Telomere	Telomere	CTC1, TERT, NBN	3	145	25	8240	6.82	0.07	1.00

ManacusMK	GOTERM_MF_DIRECT	GO:0098505~G-rich strand telomeric DNA binding	Telomere	CTC1, POT1, TERF2	3	93	5	8771	56.59	0.00	0.21
ManacusMK	GOTERM_MF_DIRECT	GO:0042162~telomeric DNA binding	Telomere	CTC1, POT1, TERF2	3	93	20	8771	14.15	0.02	0.98
ManacusMK	GOTERM_BP_DIRECT	GO:0000723~telomere maintenance	Telomere	CTC1, POT1, TERF2	3	90	29	8814	10.13	0.03	1.00
ManacusMK	UP_KEYWORDS	Telomere	Telomere	CTC1, POT1, TERF2	3	100	30	9790	9.79	0.04	1.00
ManacusMK	GOTERM_BP_DIRECT	GO:0050916~sensory perception of sweet taste	Diet	ITPR3, T1R3	2	90	4	8814	48.97	0.04	1.00
ManacusMK	GOTERM_CC_DIRECT	GO:0070187~telosome	Telomere	POT1, TERF2	2	92	5	9261	40.27	0.05	1.00
ManacusMK	GOTERM_BP_DIRECT	GO:0050917~sensory perception of umami taste	Diet	ITPR3, T1R3	2	90	5	8814	39.17	0.05	1.00
ManacusMK	GOTERM_BP_DIRECT	GO:0016233~telomere capping	Telomere	POT1, TERF2	2	90	6	8814	32.64	0.06	1.00
ManacusMK	GOTERM_MF_DIRECT	GO:0010521~telomerase inhibitor activity	Telomere	CTC1, POT1	2	93	6	8771	31.44	0.06	1.00
ManacusMK	GOTERM_CC_DIRECT	GO:0000783~nuclear telomere cap complex	Telomere	POT1, TERF2	2	92	7	9261	28.76	0.07	1.00
ManacusMK	GOTERM_BP_DIRECT	GO:0007286~spermatid development	Sperm	PIWIL1, TOPAZ1, KIT	3	90	48	8814	6.12	0.08	1.00
ManacusMK	GOTERM_BP_DIRECT	GO:0051974~negative regulation of telomerase activity	Telomere	CTC1, POT1	2	90	10	8814	19.59	0.10	1.00
ManacusMK	GOTERM_BP_DIRECT	GO:0032206~positive regulation of telomere maintenance	Telomere	TERF2, GNL3	2	90	10	8814	19.59	0.10	1.00

Table S1. Results of functional annotation and enrichment testing using DAVID. Related to Figure 2. Enriched functional database terms related to important functional categories are highlighted for key nodes in the phylogeny; relevant terms with significant enrichment ($p < 0.05$ before multiple correction) as well as terms with p-values < 0.1 are listed; terms unrelated to the five focal categories related to manakin biology (diet/sensory system/muscle/telomere/sperm) are not shown. *Count*: the number of genes under positive selection in the enriched term. *List total*: the overall number of positively selected genes annotated in the type of database, not related to this specific term. *Pop hits*: the number of genes in the analysis associated with this particular database term. *Pop total*: the total number of genes in the analysis in this database type (e.g. UP_KEYWORDS). Enrichment is a measurement of how much more frequently a particular term is represented among the significant genes than in the gene list as a whole.

Category	GO ID	GO Name	From DAVID?	# genes (manakin dataset)	Manakin genes with selection in target nodes	Genes significant in suboscines	Genes significant in Pipridae	Genes significant in Piprinae	Genes significant in McDonald-Kreitman test
Muscle	CC GO:0042383	Sarcolemma	Yes	130	8	ATP1A1,CLCN1,COL6A1	**COL6A1,COL6A3,CD5,ATP1A1,SLC2A5, CLCN1**	LAMP1	RYR3
Muscle	BP GO:0100001	Regulation of skeletal muscle contraction by action potential	No	1	1				SCN4A
Muscle	BP GO:0006936	Muscle contraction	No	113	9	CLCN1,CRYAB,MYH11	CLCN1,LMOD1,MYOM2	MYOF,MYOM2	MYH13, SCN4A
Muscle	BP GO:0003009	Skeletal muscle contraction	No	27	1			TNNC1	
Muscle	BP GO:0050905	Neuromuscular process	No	17	1				GBA
Sensory	UP_Keywords	Vision	Yes	122	16	**ADGRV1,BBS10, FAM161A,CYP4V2,RGR,RGS9, EYS,SPATA7, RPGR,CNGB1,*ROM1**	CPLX4,LCTL,CYP4V2, PDC,PDE6C	EYS	SPATA7
Sensory	BP GO:0007601	Visual perception	No	218	16	ADGRV1,BBS10,CNGB1, FAM161A,CYP4V2, ROM1,RGR,RGS9, RPGR	CPLX4,LCTL,CYP4V2, PDC,PDE6C	OAT	MYO9A, SPATA7
Sensory	BP GO:0010996	Response to auditory stimulus	No	12	0				
Sensory	BP GO:0007605	Sensory perception of sound	No	171	8	ADGRV1,ALDH7A1, GRXCR2,LOXHD1, MYO7B,WDR1	LOXHD1,SLC26A5, SLC52A3		
Diet (Taste + Digestion)	BP GO:0050916	Sensory perception of sweet taste	Yes	8	2				**ITPR3, T1R3**
Diet (Taste + Digestion)	BP GO:0050917	Sensory perception of umami taste	Yes	6	2				**ITPR3, T1R3**
Diet (Taste + Digestion)	BP GO:0050909	Sensory perception of taste	No	11	0				
Diet (Taste + Digestion)	CC GO:0005903	Brush border	Yes	57	17	**VIL1,SLC9A3,SLC15A1,MYO1B, DAB1,MME, SI,CDHR2,MYO7B, TMPRSS15**	**SLC9A3,SLC34A2,FLII,SI,LCTL**	ANKS4B, SI	ITPR3
Diet (Taste + Digestion)	CC GO:0031526	Brush border membrane	Yes	65	13	**GNA13,SLC9A3,SLC7A,GNA12, CDHR2,SLC3A1,SLC5A1, MFSD10,ACE2,AMN,SLC28A2**	ABCC2,SLC34A2, SLC9A3	SLC26A3	ABCC2
Diet (Taste + Digestion)	BP GO:0005975	Carbohydrate metabolic process	Yes	115	15	A4GNT,GALM,GUSB, HYAL2,LPH,SI,MAN1C1,SHPK, SLC3A1	**LDHB,SLC35A1,SI,LPH, NAGPA,SLC2A5,SIAE,LCTL**	SI	
Diet (Taste + Digestion)	BP GO:0015755	Fructose transport	Yes	6	2		**SLC2A5,SLC26A5**		
Diet (Taste + Digestion)	BP GO:0044245	Polysaccharide digestion	Yes	5	2	SI,LPH	**SI,LPH**	SI	
Diet (Taste + Digestion)	BP GO:0042159	lipoprotein catabolic process	Yes	5	3	CTSD	**ATM,APOB**		
Diet (Taste +	BP GO:0008643	Carbohydrate transport	Yes	21	3		**SLC35A1,SLC35D2,**		

Digestion)							**SLC2A5**		
Diet (Taste + Digestion)	BP GO:0030073	insulin secretion	Yes	30	4	FAM3B	**SNX19,GPR119,FAM3B**	GPR119, RAPGEF4	
Diet (Taste + Digestion)	KEGG hsa04973	Carbohydrate digestion and absorption	Yes	38	7	**HK3,SI,SLC5A1,ATP1A1, LPH,PLCB1**	**SI,ATP1A1,LPH, SLC2A5**	SI	T1R3
Diet (Taste + Digestion)	KEGG hsa04975	Fat digestion and absorption	No	40	4	ACAT1,FABP2,PLPP3	APOB		
Diet (Taste + Digestion)	KEGG hsa04974	Protein digestion and absorption	Yes	95	18	**DPP4,SLC9A3,ACE2, COL3A1,SLC15A1,CTRLMME, SLC7A9,COL6A1, SLC3A1,ATP1A1**	**SLC9A3,COL3A1, COL15A1,CTRL, COL4A1, COL12A1,COL6A1, COL6A3,ATP1A1**		COL1A2, PGA5, SLC16A10
Telomeres	UP_Keywords	Telomere	Yes	41	11	PINX1,SETX,SMC5, SMC6,TERT	NSMCE2,TERB1	**CTC1,TERT,NBN**	**CTC1, POT1, TERF2**
Telomeres	CC GO:0000781	Chromosome, telomeric region	Yes	207	21	**SETX,TERT,DOT1L, DYDC2,SMC5,TP53BP1,SMC6, CBX3,DDB1, PINX1,PRKDC,SMCHD1**	**TERB1,NSMCE2,ATM,TP53 BP1,CBX3,MCM3,NSMCE2**	**TERT,SPO11, TP53BP1,NBN, CTC1,**	CTC1, POT1, TERF2
Telomeres	BP GO:0000723	Telomere maintenance	Yes	66	6	PRKDC,TERT		TERT,NBN,CTC1	**CTC1, POT1, TERF2**
Telomeres	BP GO:0016233	Telomere capping	Yes	28	4	PRKDC		CTC1	**POT1, TERF2, CTC1**
Telomeres	BP GO:0051974	Negative regulation of telomerase activity	Yes	22	3	PINX1		CTC1	**CTC1, POT1**
Telomeres	BP GO:0032206	Positive regulation of telomere maintenance	Yes	14	3			NBN	**TERF2, GNL3**
Telomeres	CC GO:0070187	Telosome	Yes	23	3		TERB1		**POT1, TERF2**
Telomeres	CC GO:0000783	Nuclear telomere cap complex	Yes	14	3	TERT		TERT	**POT1, TERF2**
Telomeres	MF GO:0042162	Telomeric DNA binding	Yes	53	5	TERT,TP53BP1	TP53BP1	CTC1,TERT, TP53BP1	**CTC1, POT1, TERF2**
Telomeres	MF GO:0010521	Telomerase inhibitor activity	Yes	18	3	PINX1		CTC1	**CTC1, POT1**
Telomeres	MF GO:0098505	G-rich strand telomeric DNA binding	Yes	21	3			CTC1	**CTC1, POT1,TERF2**
Sperm	UP_Keywords	Spermatogenesis	Yes	141	18	**TDRD1,SETX,DAZAP1, SLCO4C1,ASZ1,TDRD12, MYCBPAP,TDRD6, SPATA20,CFAP54, DLEC1**	ADAD1,DLEC1,LRGUK	ASZ1,SUN5, TDRD1	CADM1, PIWIL1, PIWIL2, TOPAZ1
Sperm	BP GO:0007283	Spermatogenesis	No	281	23	ACE,ADAM10,ASZ1, CFAP54,E2F1,GGT5, MYCBPAP,PTTG1,SETX, SLCO4C1,TDRD1, TDRD12,TDRD6	APOB,GGT5,LRGUK, PTTG1,TSPAN8	ASZ1,SUN5, SPO11,TDRD1	CADM1, CNR1,KIT,PIWIL1 ,PIWIL2
Sperm	BP GO:0007286	Spermatid development	Yes	69	9	RSPH1	ADAD1	JAM2,SUN5,SPO11	**KIT, CCDC42, PIWIL1,**

								TOPAZ1
Sperm	CC GO:0036126	Sperm flagellum	No	47	6	ATP1A1, DNAH17, RPGR	ATP1A1,CFAP65, SAXO2	DNAH8
Sperm	CC GO:0061827	Sperm head	No	5	0			
Pigmentation	BP GO:0006582	Melanin metabolic process	No	1	1	BCL2		
Pigmentation	BP GO:0051875	Pigment granule localization	No	0				
Pigmentation	BP GO:0050931	Pigment cell differentiation	No	0				
Pigmentation	BP GO:0032438	Melanosome organization	No	34	0			
Pigmentation	MF GO:0031779	Melanocortin receptor binding	No	2	0			
Pigmentation	BP GO:0048023	Positive regulation of melanin biosynthesis	No	7	0			
Pigmentation	BP GO:0032402	Melanosome transport	No	22	0			
Pigmentation	BP GO:0042438	Melanin biosynthetic process	No	14	0			

Table S2. Positively selected genes associated with main functional categories. Related to Figure 2. We collected functional database (GO, KEGG and UP) terms associated with five broad categories related to manakin biology (diet-related genes, including taste and digestion; muscle-related genes, sensory genes (vision and audition), telomere-related genes and sperm-related genes) and listed the positively selected genes within each database term. Genes in a term that are identified by DAVID as having an enrichment tendency ($p < 0.1$, Table S1) are shown in bold. Functional databases: CC_GO - Cellular Component Gene Ontology; BP_GO - Biological Process Gene Ontology; MF_GO - Molecular Function Gene Ontology; UP_keywords - UniProt Keywords; KEGG - Kyoto Encyclopedia of Genes and Genomes. Asterisk indicates an instance (*ROM1*) where later versions of the UP_Keyword database included a gene that was not associated with that particular term in the version of DAVID used at the time of analysis.

# manakin-divergent UCNEs near genes	Gene ID	Gene name	# UCNEs analyzed for index	UCNEs with more changes in Piprinae	UCNEs with more changes in Pipridae
10	NR2F1	nuclear receptor subfamily 2 group F member 1(NR2F1)	7	1	6
7	TLE4	TLE family member 4, transcriptional corepressor(TLE4)	7	4	2
7	TCF4	transcription factor 4(TCF4)	1		
5	NR4A2	nuclear receptor subfamily 4 group A member 2(NR4A2)	3		3
5	ZC3H3	zinc finger CCCH-type containing 3(ZC3H3)	1		1
4	SHOX2	short stature homeobox 2(SHOX2)	4		3
2	BCL11A	BAF chromatin remodeling complex subunit BCL11A(BCL11A)	2		2
2	PBX3	PBX homeobox 3(PBX3)	1	1	
2	SMAD3	SMAD family member 3(SMAD3)	0		
2	TBX2	T-box transcription factor 2(TBX2)	2		2
2	FOXD3	forkhead box D3(FOXD3)	2		1
2	NEUROD6	neuronal differentiation 6(NEUROD6)	2	1	1
1	DCAF12L2	DDB1 and CUL4 associated factor 12 like 2(DCAF12L2)	1		1
1	EBF2	EBF transcription factor 2(EBF2)	1	-	-
1	EBF3	EBF transcription factor 3(EBF3)	0		
1	FBXO8	F-box protein 8(FBXO8)	1		1
1	ISL1	ISL LIM homeobox 1(ISL1)	1		1
1	MEIS2	Meis homeobox 2(MEIS2)	1	-	-
1	POU3F2	POU class 3 homeobox 2(POU3F2)	1		1
1	POU6F2	POU class 6 homeobox 2(POU6F2)	1	1	
1	SOX3	SRY-box transcription factor 3(SOX3)	1		1
1	TLX3	T cell leukemia homeobox 3(TLX3)	1		1
1	TNFAIP3	TNF alpha induced protein 3(TNFAIP3)	1	-	-
1	ANXA1	annexin A1(ANXA1)	1		1
1	BNC2	basonuclin 2(BNC2)	1		1
1	DACH2	dachshund family transcription factor 2(DACH2)	1	-	-
1	DRGX	dorsal root ganglia homeobox(DRGX)	1		1
1	FOXP2	forkhead box P2(FOXP2)	1		1
1	GBX2	gastrulation brain homeobox 2(GBX2)	1		1
1	ID4	inhibitor of DNA binding 4, HLH protein(ID4)	1	-	-
1	MBD5	methyl-CpG binding domain protein 5(MBD5)	1		1
1	MBNL1	muscleblind like splicing regulator 1(MBNL1)	1	-	-
1	NPAS3	neuronal PAS domain protein 3(NPAS3)	1	-	-
1	NFIB	nuclear factor I B(NFIB)	1	1	
1	ONECUT2	one cut homeobox 2(ONECUT2)	0		
1	OTP	orthopedia homeobox(OTP)	1	-	-
1	PAX1	paired box 1(PAX1)	1		1
1	PAX5	paired box 5(PAX5)	1	1	
1	PAX6	paired box 6(PAX6)	1		1
1	PAX9	paired box 9(PAX9)	1		1
1	SALL3	spalt like transcription factor 3(SALL3)	0		
1	TSHZ3	teashirt zinc finger homeobox 3(TSHZ3)	0		

1	TNPO1	transportin 1(TNPO1)	1		1
1	ZEB2	zinc finger E-box binding homeobox 2(ZEB2)	0		
1	IRXB	iroquois homeobox gene cluster (IRX5 and IRX6)	1	-	-
1	MIR4307	MicroRNA 4307 (MIR4307)	1	1	
1	LPHN2	Latrophilin 2 (LPHN2)	1		1
1	ODZ3	Teneurin-3 (ODZ3)	1	-	-

Table S3. Genes proximal to ultra-conserved non-coding elements (UCNEs) accelerated in manakins. Related to Figure 2. Of the 99 manakin-accelerated UCNEs, proximal genes were identified to 86 elements; the numbers in parentheses in the first column refers to the number of UCNEs for that locus. For a subset of the set of 99 elements (74 elements, 63 associated with genes), the number of changes on the branch leading to Pipridae and Piprinae were counted, and the number of accelerated elements in either class is listed. 14 elements had more changes in Piprinae (11 associated with genes; and 3 that were not close to an identified locus); 46 elements had relatively more changes in Pipridae, including 8 elements not associated with genes. 14 elements had equal number of changes (or no changes on either ancestral branch); these are indicated by '-' if only a single element is proximal to a gene; for *TLE4*, one of the set of accelerated elements also had an equal number of changes, and for *SHOX2*, *TCF4* and *FOXD3*, one element also did not have changes on either ancestral branch.

Clade (# on Fig S5D)	# Taxa	Bi-parental care	Male color optima	Female color optima	Fruit optima	Support	Pseudo count	Notes
Philepitta asities (1)	2	1	61.3513	40.6335	58.5194	851	80	Described as lekking, and lacking biparental care (but males of both species are frequently seen around nests).
Calyptomena broadbills (2)	3	0	53.4917	48.8808	85.8928	5	147	Biparental care; brightly colored males and females
Manakins (3)	46	1	52.5552	39.9517	74.9475	953	68	All lack biparental care, most (not all) have bright males and dully colored females
Cotingas (4)	60	0	55.6063	48.6246	82.8966	5	50	Not all downstream taxa lack biparental care--clades with biparental care also have brightly colored females
Mionectes (5)	5	1	45.7588	45.0649	69.1945	975	71	lekking
Tyrannids (6)	380	0	46.7528	46.3586	7.2022	47	128	Most, but not all downstream taxa have biparental care (except for *Mionectes* and possibly *Cnipodectes*)

Table S4. Summary of integrated method combining shifts in biparental care with shifts in fruit and plumage. Related to Figure 5. The method combines shifts in discrete data (loss of biparental care: 1; gain of biparental care: 0) with shifts in continuous traits (fruit, male and female plumage color; optima are from the PhylogeneticEM analysis of all three traits combined). Six concordant shifts in breeding system and fruit/plumage were detected; support values refer to the number of character maps (out of 1000) in which a concordant shift was detected. Thus, for example, across 1000 stochastic character maps simulating the evolutionary history of parental care in suboscines, conditioned on the observed tip values for parental care, in 851 of these a loss of biparental care was inferred in *Philepitta*. Pseudo.count denotes number of times a shift was detected in the null distribution: for example, across 1000 stochastic character maps conditioned only on the inferred transition matrix, in 147 of these a loss of biparental care was inferred in *Calyptomena*. Number of downstream taxa for each shift are shown. Natural history notes from[S20].

References

S1. Karten, H.J., Brzozowska-Prechtl, A., Lovell, P.V., Tang, D.D., Mello, C.V., Wang, H., and Mitra, P.P. (2013). Digital atlas of the zebra finch (Taeniopygia guttata) brain: a high-resolution photo atlas. J. Comp. Neurol. *521*, 3702–3715. https://doi.org/10.1002/cne.23443.

S2. Luksch, H. (2003). Cytoarchitecture of the avian optic tectum: neuronal substrate for cellular computation. Rev. Neurosci. *14*, 85–106. https://doi.org/10.1515/revneuro.2003.14.1-2.85.

S3. Isa, T., Marquez-Legorreta, E., Grillner, S., and Scott, E.K. (2021). The tectum/superior colliculus as the vertebrate solution for spatial sensory integration and action. Curr. Biol. *31*, R741–R762. https://doi.org/10.1016/j.cub.2021.04.001.

S4. Luksch, H., Cox, K., and Karten, H.J. (1998). Bottlebrush dendritic endings and large dendritic fields: Motion‐detecting neurons in the tectofugal pathway. J. Comp. Neurol. *396*, 399–414. https://doi.org/10.1002/(sici)1096-9861(19980706)396:3<399::aid-cne9>3.3.co;2-r.

S5. Wylie, D.R.W., Gutierrez-Ibanez, C., Pakan, J.M.P., and Iwaniuk, A.N. (2009). The optic tectum of birds: mapping our way to understanding visual processing. Can. J. Exp. Psychol. *63*, 328–338. https://doi.org/10.1037/a0016826.

S6. Agoston, Z., and Schulte, D. (2009). Meis2 competes with the Groucho co-repressor Tle4 for binding to Otx2 and specifies tectal fate without induction of a secondary midbrain-hindbrain boundary organizer. Development *136*, 3311–3322. https://doi.org/10.1242/dev.037770.

S7. Pease, J.B., Driver, R.J., de la Cerda, D.A., Day, L.B., Lindsay, W.R., Schlinger, B.A., Schuppe, E.R., Balakrishnan, C.N., and Fuxjager, M.J. (2022). Layered evolution of gene expression in “superfast” muscles for courtship. Proc. Natl. Acad. Sci. U. S. A. *119*, e2119671119. https://doi.org/10.1073/pnas.2119671119.

S8. Toda, Y., Ko, M.-C., Liang, Q., Miller, E.T., Rico-Guevara, A., Nakagita, T., Sakakibara, A., Uemura, K., Sackton, T., Hayakawa, T., et al. (2021). Early origin of sweet perception in the songbird radiation. Science *373*, 226–231. https://doi.org/10.1126/science.abf6505.

S9. Zhang, F., Klebansky, B., Fine, R.M., Xu, H., Pronin, A., Liu, H., Tachdjian, C., and Li, X. (2008). Molecular mechanism for the umami taste synergism. Proc. Natl. Acad. Sci. U. S. A. *105*, 20930–20934. https://doi.org/10.1073/pnas.0810174106.

S10. Winnig, M., Bufe, B., Kratochwil, N.A., Slack, J.P., and Meyerhof, W. (2007). The binding site for neohesperidin dihydrochalcone at the human sweet taste receptor. BMC Struct. Biol. *7*, 66. https://doi.org/10.1186/1472-6807-7-66.

S11. Jiang, P., Cui, M., Zhao, B., Snyder, L.A., Benard, L.M.J., Osman, R., Max, M., and Margolskee, R.F. (2005). Identification of the cyclamate interaction site within the transmembrane domain of the human sweet taste receptor subunit T1R3. J. Biol. Chem. *280*, 34296–34305. https://doi.org/10.1074/jbc.M505255200.

S12. Jiang, P., Cui, M., Zhao, B., Liu, Z., Snyder, L.A., Benard, L.M.J., Osman, R., Margolskee,

R.F., and Max, M. (2005). Lactisole interacts with the transmembrane domains of human T1R3 to inhibit sweet taste. J. Biol. Chem. *280*, 15238–15246. https://doi.org/10.1074/jbc.M414287200.

S13. Pizo, M.A., Morales, J.M., Ovaskainen, O., and Carlo, T.A. (2021). Frugivory specialization in birds and fruit chemistry structure mutualistic networks across the Neotropics. Am. Nat. *197*, 236–249. https://doi.org/10.1086/712381.

S14. Herrera, C.M. (1987). Vertebrate-dispersed plants of the Iberian Peninsula: A study of fruit characteristics. Ecol. Monogr. *57*, 305–331. https://doi.org/10.2307/2937089.

S15. Jordano, P. (1995). Angiosperm fleshy fruits and seed dispersers: A comparative analysis of adaptation and constraints in plant-animal interactions. Am. Nat. *145*, 163–191. https://doi.org/10.1086/285735.

S16. Corlett, R.T. (1996). Characteristics of vertebrate-dispersed fruits in Hong Kong. J. Trop. Ecol. *12*, 819–833. https://doi.org/10.1017/s0266467400010075.

S17. Galetti, M., Pizo, M.A., and Morellato, L.P.C. (2011). Diversity of functional traits of fleshy fruits in a species-rich Atlantic rain forest. Biota Neotrop. *11*, 181–193. https://doi.org/10.1590/s1676-06032011000100019.

S18. Potter, J.H.T., Drinkwater, R., Davies, K.T.J., Nesi, N., Lim, M.C.W., Yohe, L.R., Chi, H., Zhang, X., Levantis, I., Lim, B.K., et al. (2021). Nectar-feeding bats and birds show parallel molecular adaptations in sugar metabolism enzymes. Curr. Biol. *31*, 4667–4674.e6. https://doi.org/10.1016/j.cub.2021.08.018.

S19. Wilman, H., Belmaker, J., Simpson, J., de la Rosa, C., Rivadeneira, M.M., and Jetz, W. (2014). EltonTraits 1.0: Species-level foraging attributes of the world's birds and mammals. Ecology *95*, 2027–2027. https://doi.org/10.1890/13-1917.1.

S20. Birds of the World (2022). Comprehensive life histories for all bird species and families.